Electronic Supplementary Material (ESI) for Journal of Materials Chemistry A.

Supporting Information

Influence of the Stoichiometry of tin-based 2D/3D Perovskite active layer on Solar Cells performances

Shuyan Shao[*,a], Maykel Nijenhuis[a], Jingjin Dong[b], Simon Kahmann[a], Gert H. ten Brink[c], Giuseppe Portale[b], Maria Antonietta Loi*[*,a]*

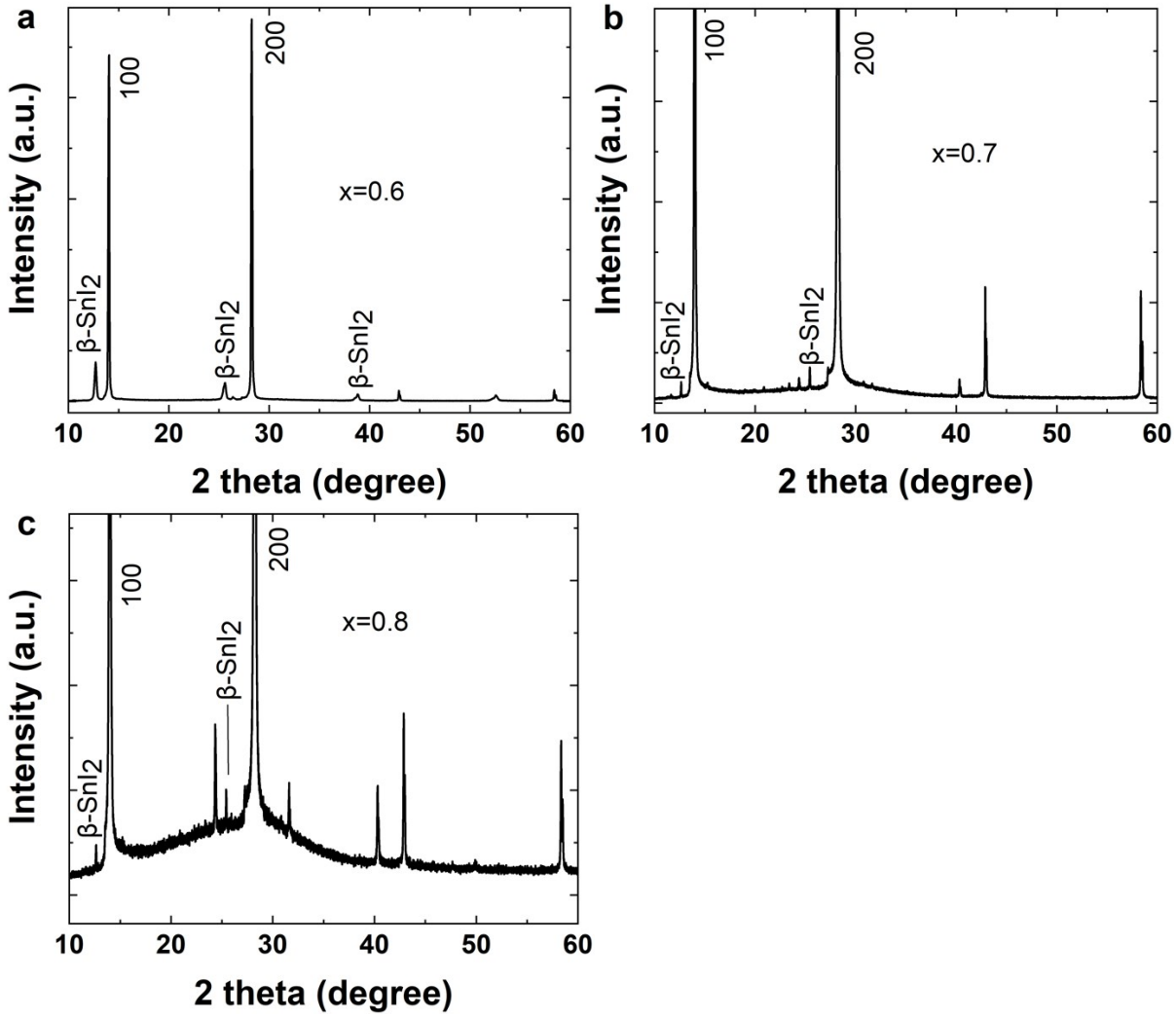

Figure S1. XRD patterns of (a) a $PEA_{0.08}FA_{0.6}SnI_3$ film with hexagonal SnI_2 (β-SnI_2) peaks at 12.7◦ , 25.6◦, and 38.8◦, (b) a $PEA_{0.08}FA_{0.7}SnI_3$ film with β-SnI_2 peaks at 12.7◦ and 25.6◦ and (c) a $PEA_{0.08}FA_{0.8}SnI_3$ film with β-SnI_2 peaks at 12.7◦ and 25.6 as well [1].

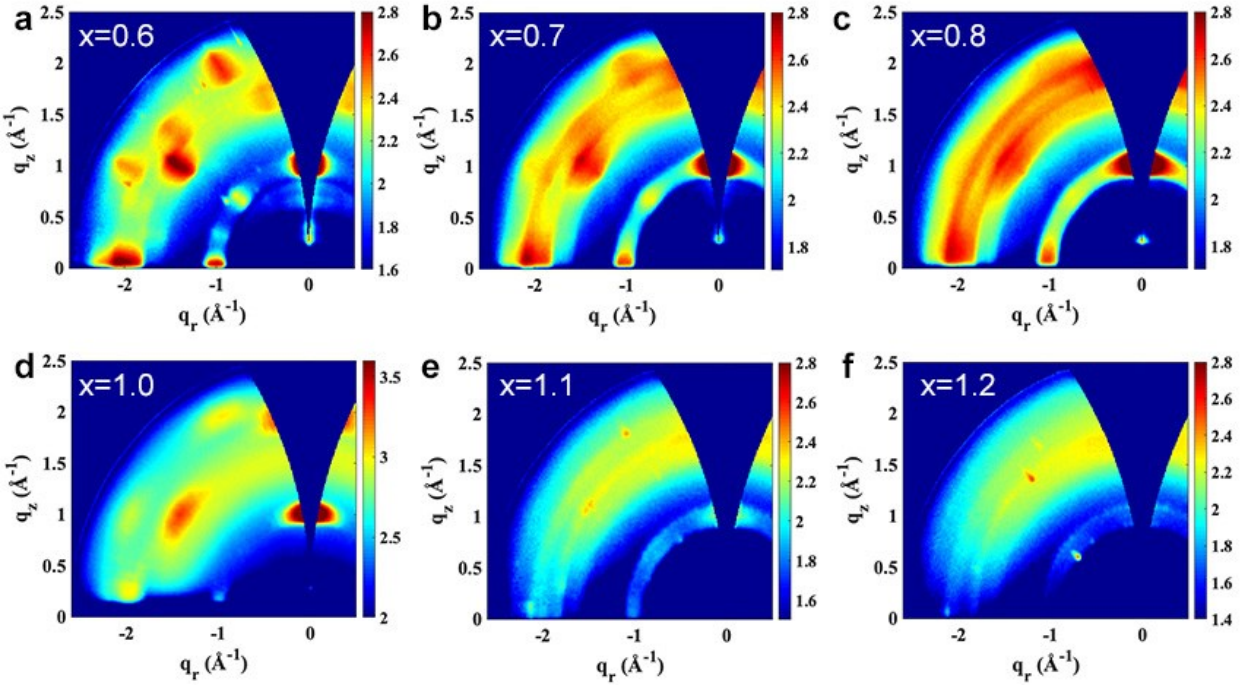

Figure S2. GIWAXS patterns of $PEA_{0.08}FA_{(x)}SnI_3$ films. The images were recorded using an incident angle of 0.25°.

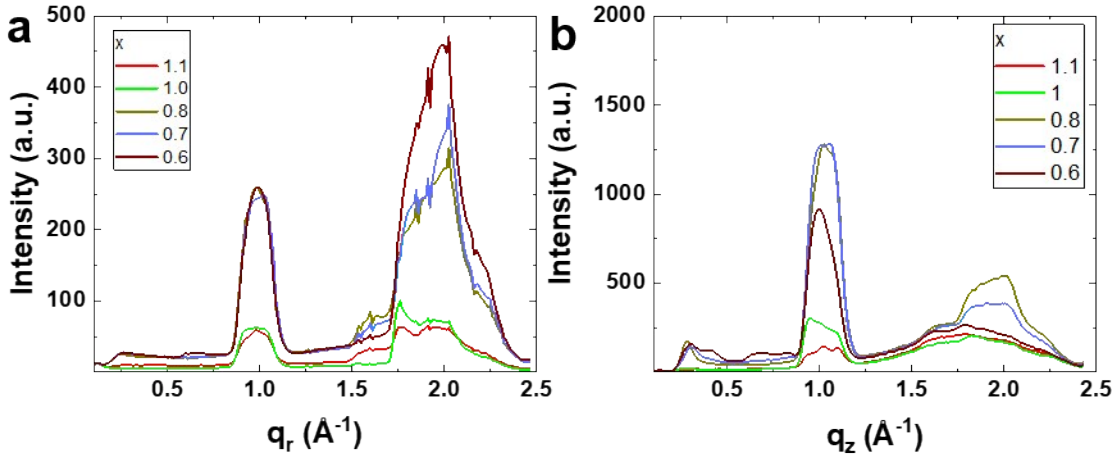

Figure S3. The line-cut data in (a) in-plane (q_z) and (b) out-of-plane (q_y) of the GIWAXS images of the $PEA_{0.08}FA_xSnI_3$ films with X-ray incident angle of 0.25°, respectively.

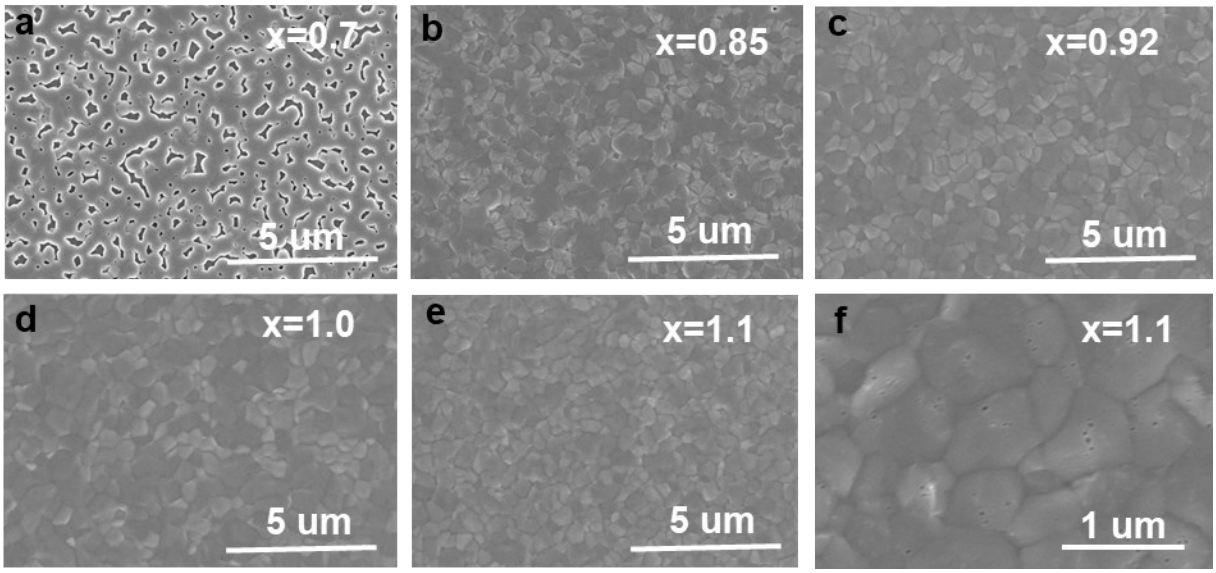

Figure S4. SEM images of the $PEA_{0.08}FA_xSnI_3$ films: (a) x=0.7, (b) x=0.85, (c) x=0.92, (d) x=1.0, (e) x=1.1, (f) the magnified image of x=1.1 sample.

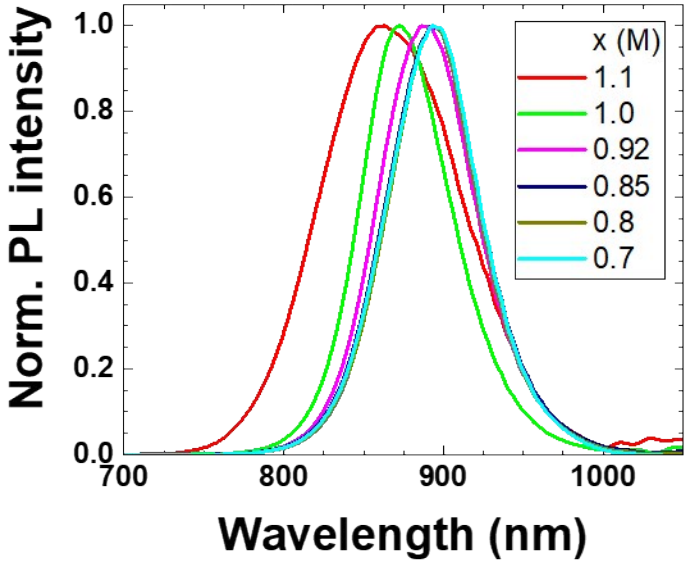

Figure S5. Normalized PL spectra of $PEA_{0.08}FA_{(x)}SnI_3$ films.

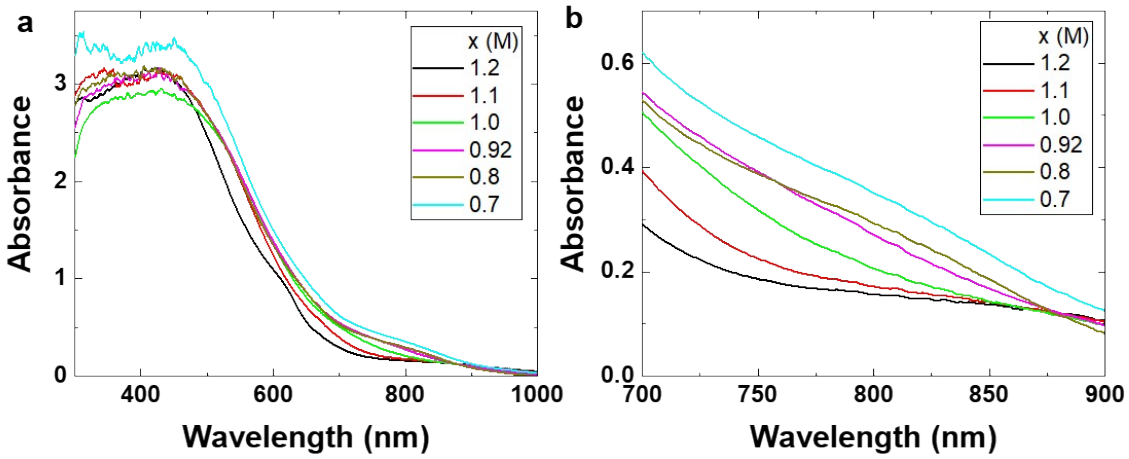

Figure S6. Absorbance of $PEA_{0.08}FA_{(x)}SnI_3$ films (a) with an incident light wavelength from 350 nm to 1000 nm and (b) from 700 nm to 900 nm. Note: the absorbance spectra in the short wavelength region (<600 nm) are saturated.

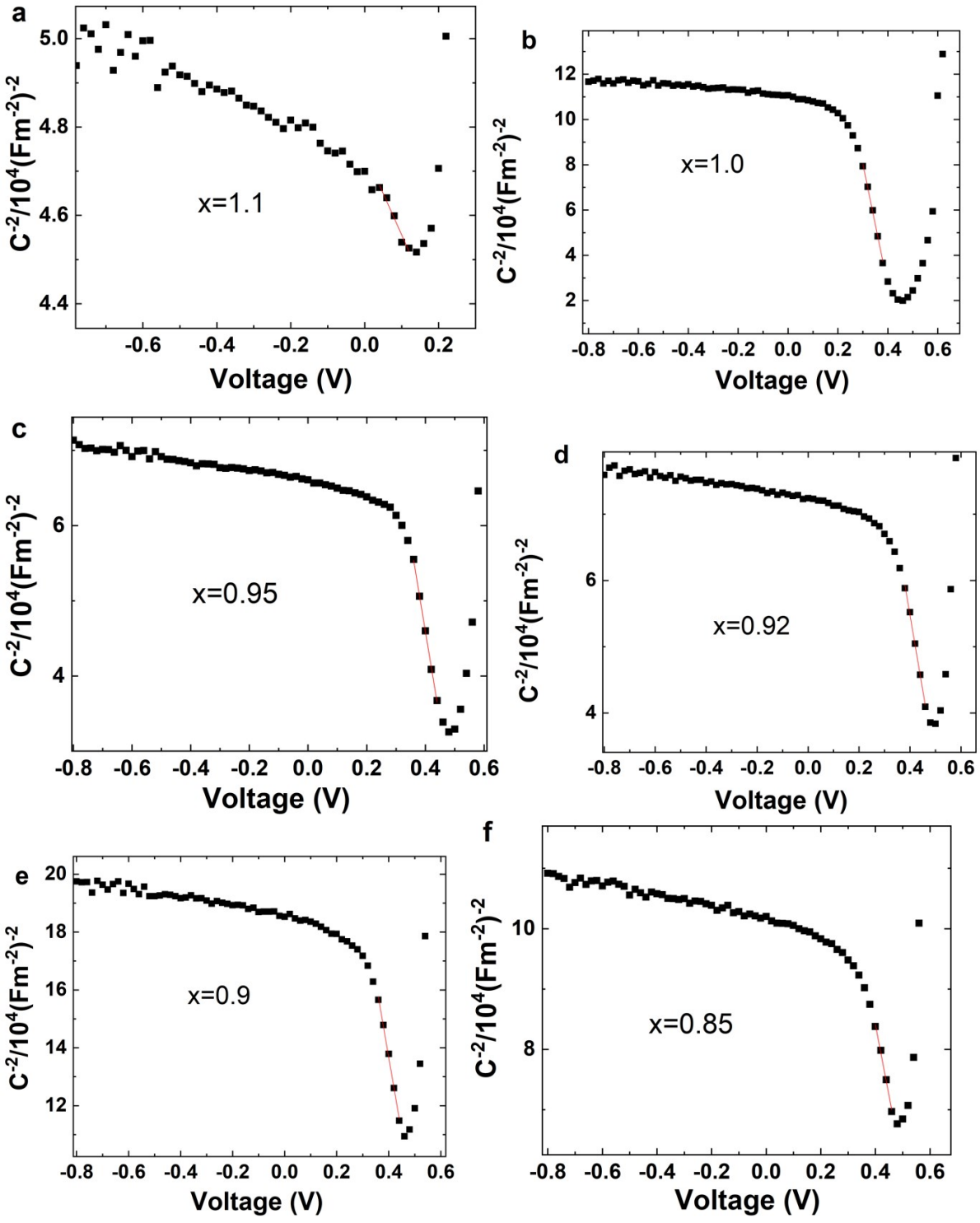
a
x=1.1
$C^{-2}/10^4(Fm^{-2})^{-2}$
Voltage (V)
b
x=1.0
$C^{-2}/10^4(Fm^{-2})^{-2}$
Voltage (V)
c
x=0.95
$C^{-2}/10^4(Fm^{-2})^{-2}$
Voltage (V)
d
x=0.92
$C^{-2}/10^4(Fm^{-2})^{-2}$
Voltage (V)
e
x=0.9
$C^{-2}/10^4(Fm^{-2})^{-2}$
Voltage (V)
f
x=0.85
$C^{-2}/10^4(Fm^{-2})^{-2}$
Voltage (V)

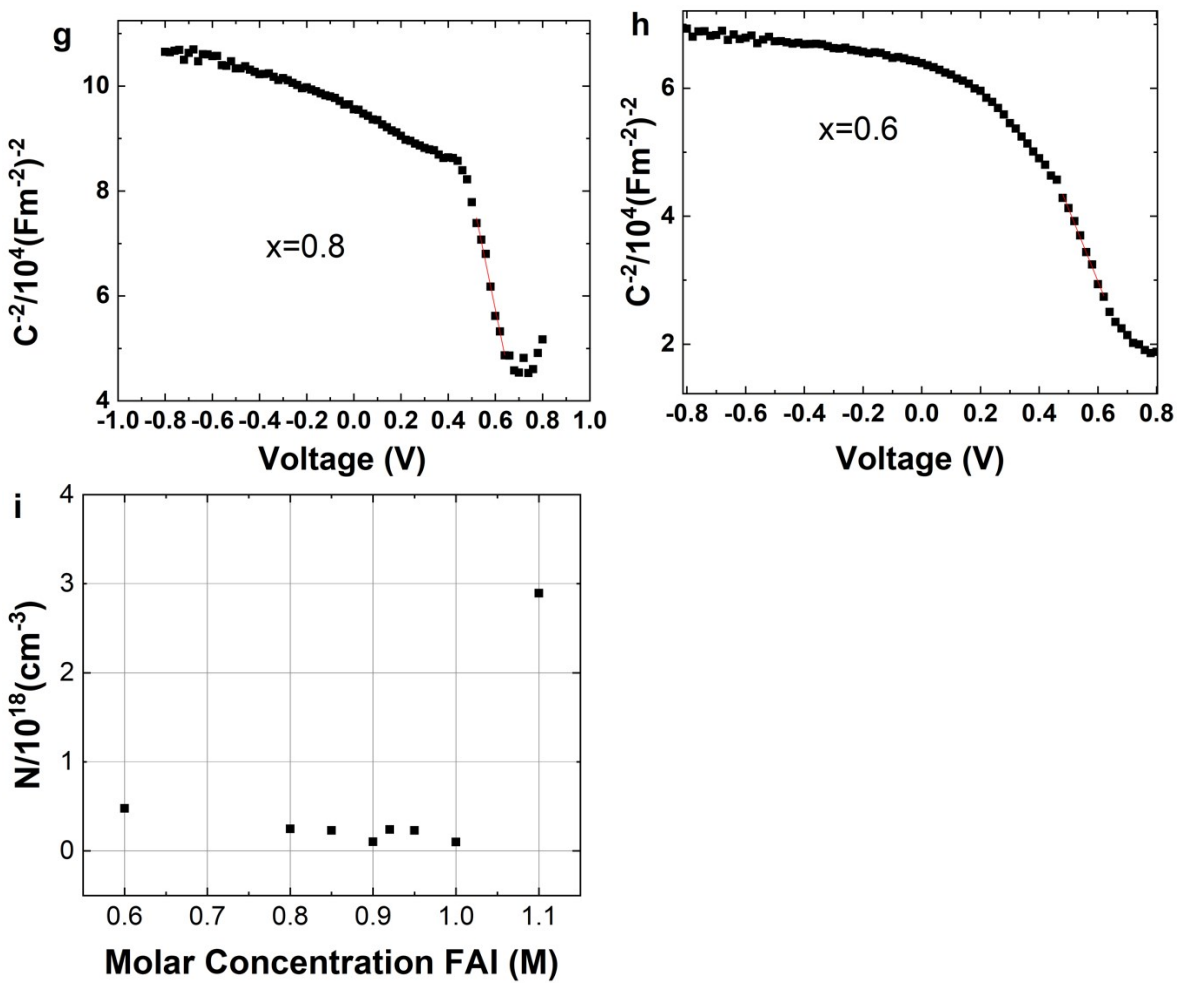

Figure S7. Mott-Schottky analysis of perovskite solar cells of different stoichiometry. (a-h) C^{-2} as a function of bias voltage. (i) carrier concentration as deriveved from Mott-Schottky analysis for the different samples.

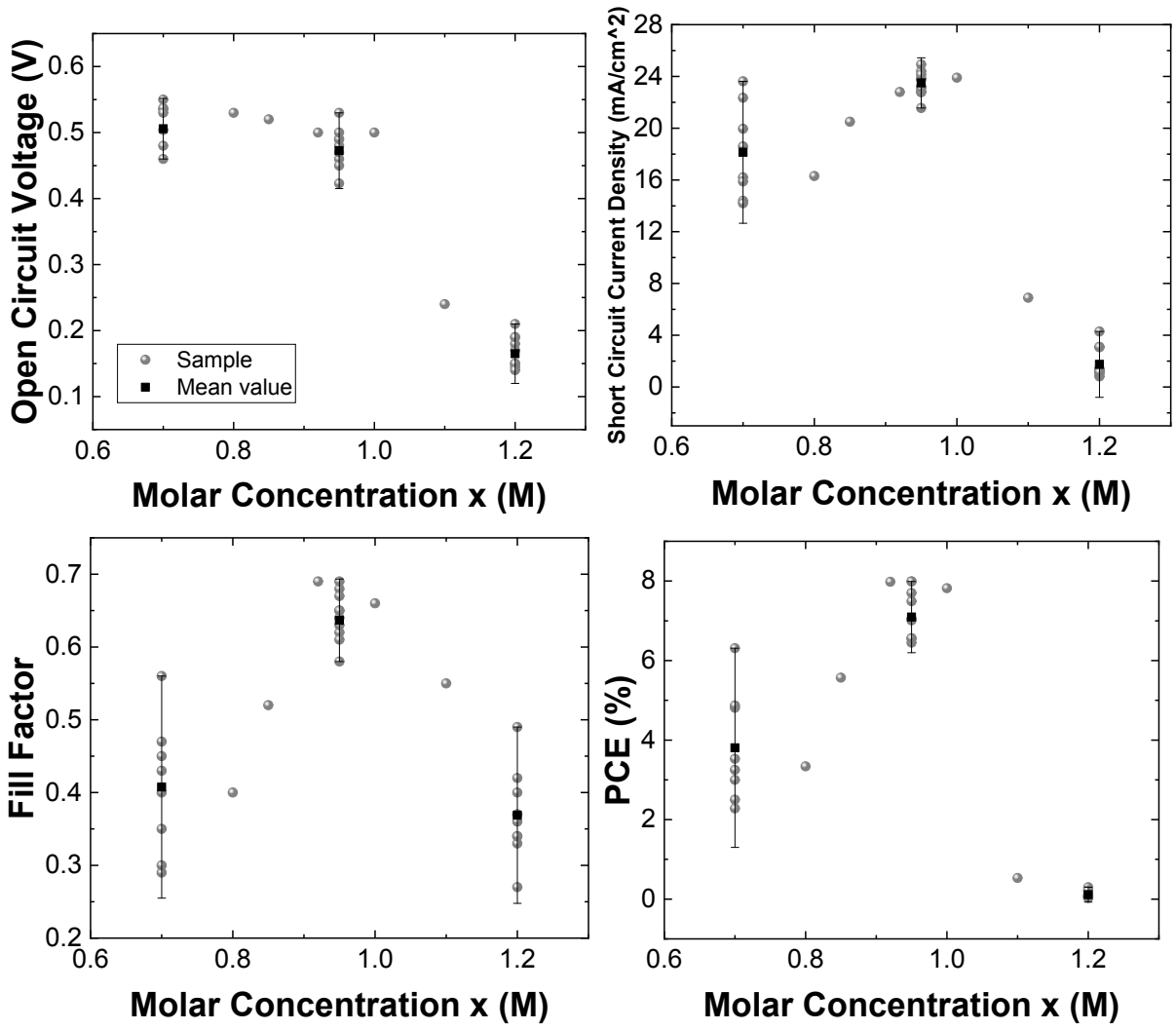

Figure S8. Statistics for V_{OC}, J_{SC}, FF and PCE of devices with an active area of 0.04 cm^2. Note that: for the 0.70 M composition 8 samples were measured, for the 0.95 M composition 9 samples, and for the 1.20 M composition also 9 samples were measured. The graph includes the values from Table 1.

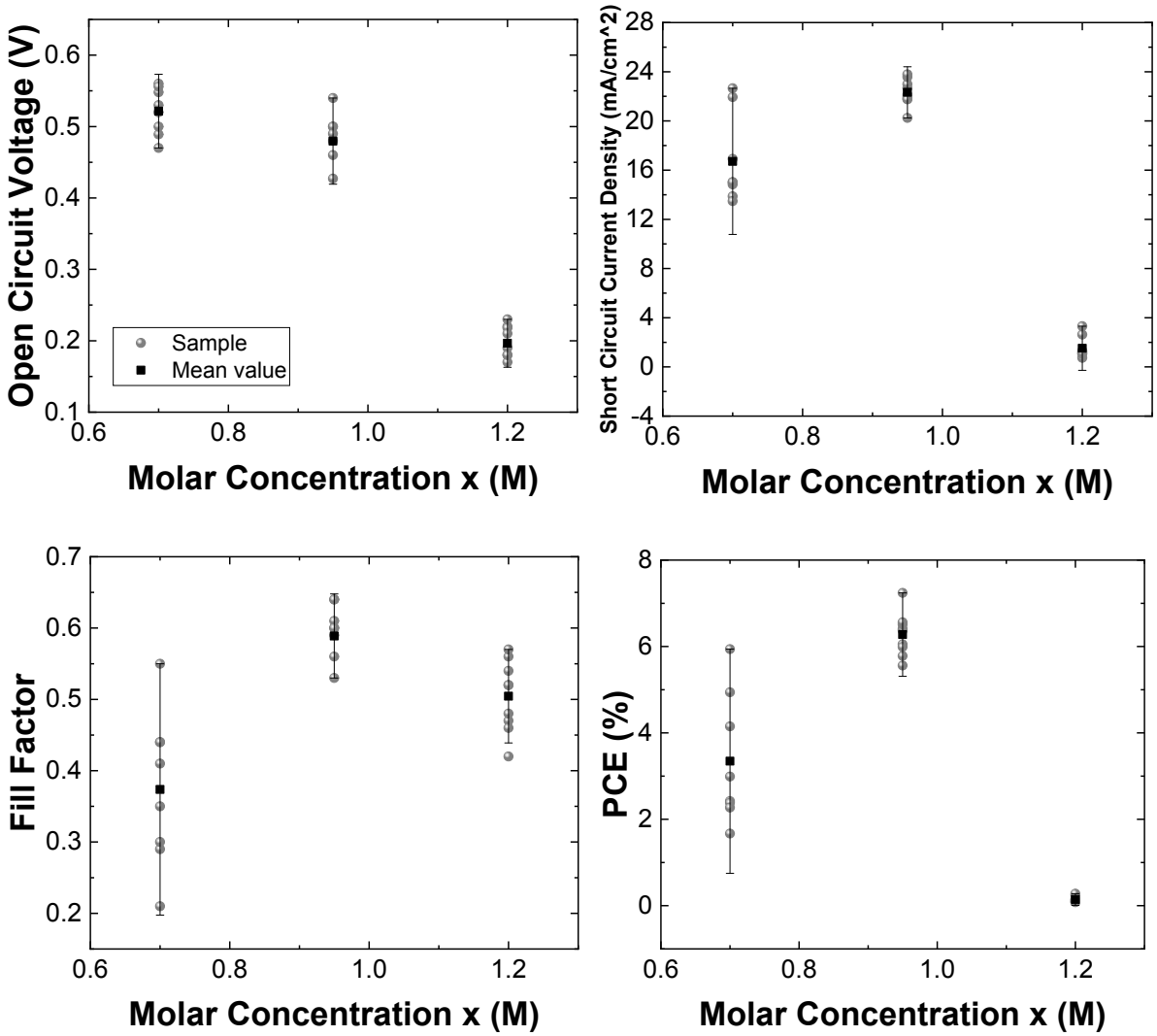

Figure S9. Statistics for V_{OC}, J_{SC}, FF and PCE of devices with an active area of 0.09 cm^2. Note that: for the 0.70 M composition 8 samples were measured, for the 0.95 M composition 9 samples, and also for the 1.20 M composition 9 samples were measured.

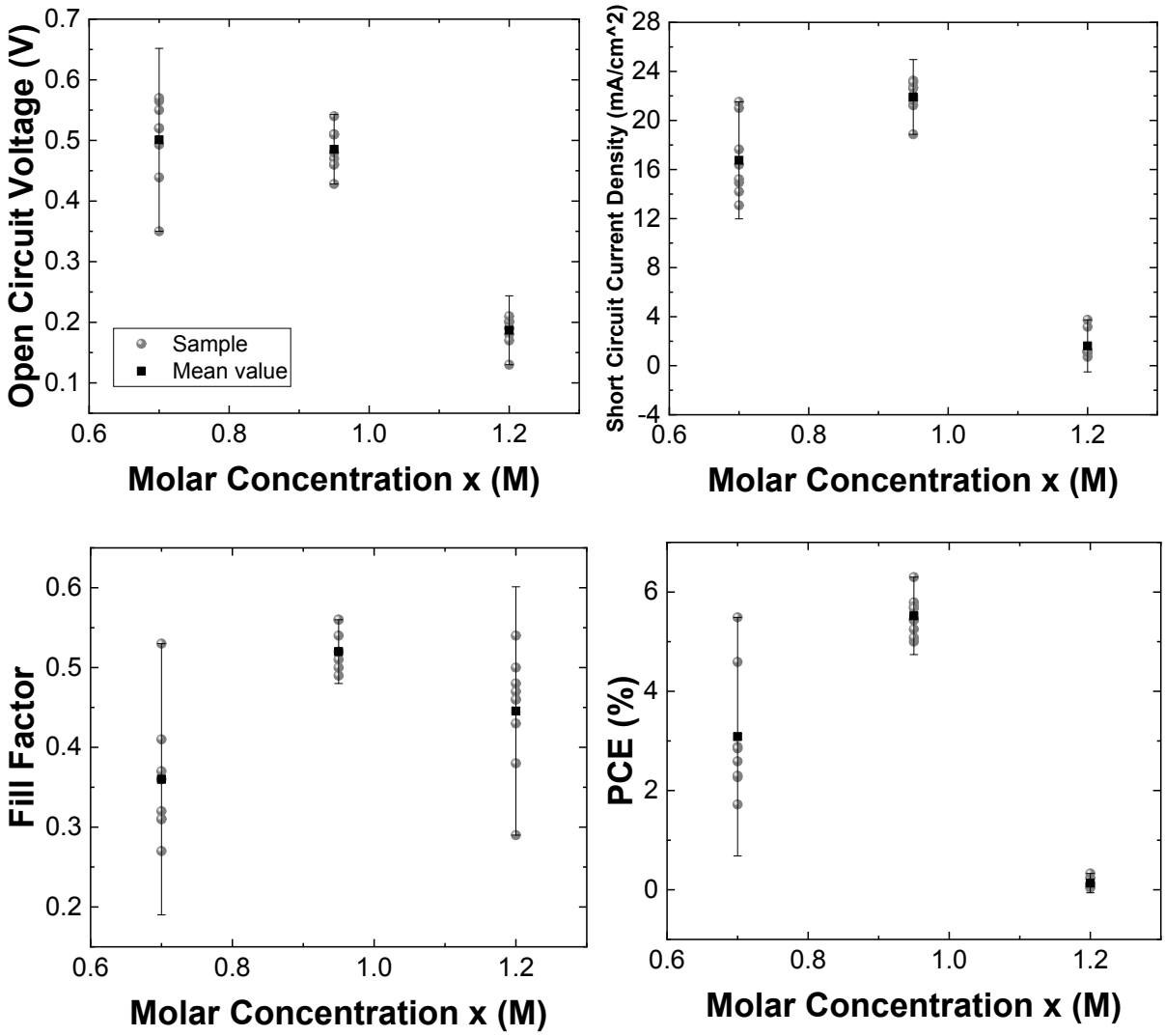

Figure S10. Statistics for V_{OC}, J_{SC}, FF and PCE of devices using different 2D/3D films with an active area of 0.25 cm^2. Note that: for the 0.70 M composition 8 samples were measured, for the 0.95 M composition 9 samples, and also for the 1.20 M composition 9 samples were measured.

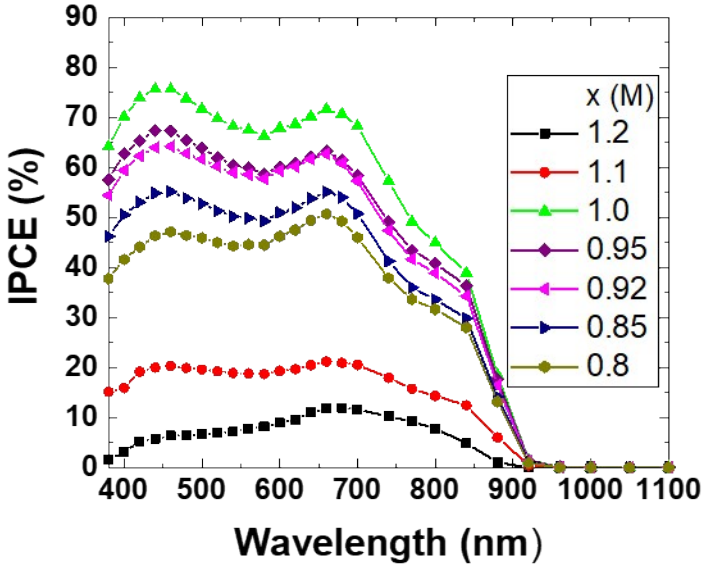

Figure S11. IPCE measurements of ITO/PEDOT:PSS/ $PEA_{0.08}FA_{(x)}SnI_3$/C60/BCP/Al devices.

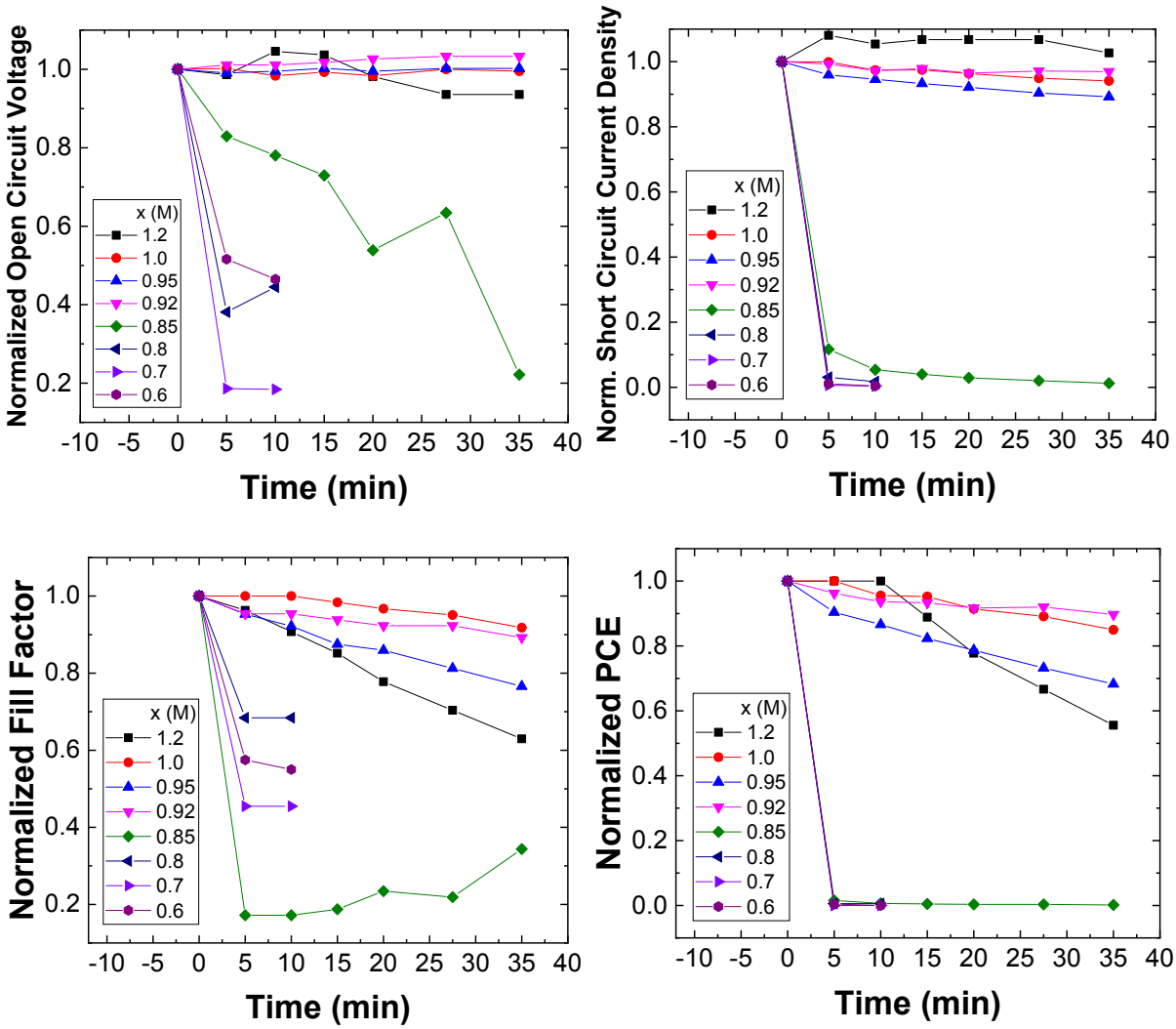

Figure 12. Variation of the V_{OC}, J_{SC}, FF and PCE of devices using different 2D/3D films vs time they have been exposed to air.

References:

[1] V. S. Kostko, O. V Kostko, G. I. Makovetskii and K. I. Yanushkevich, *Phys. status solidi*, 2002, **229**, 1349–1352.